

See discussions, stats, and author profiles for this publication at: <https://www.researchgate.net/publication/51744779>

Coenzyme A Binding to the Aminoglycoside Acetyltransferase (3)-IIIb Increases Conformational Sampling of Antibiotic Binding Site

ARTICLE *in* BIOCHEMISTRY · DECEMBER 2011

Impact Factor: 3.02 · DOI: 10.1021/bi201008f · Source: PubMed

CITATIONS

6

READS

25

4 AUTHORS, INCLUDING:



Jerome Baudry

University of Tennessee

60 PUBLICATIONS 1,728 CITATIONS

[SEE PROFILE](#)



Engin H. Serpersu

University of Tennessee

86 PUBLICATIONS 1,733 CITATIONS

[SEE PROFILE](#)

Coenzyme A Binding to the Aminoglycoside Acetyltransferase (3)-IIIb Increases Conformational Sampling of Antibiotic Binding Site

Xiaohu Hu,^{†,‡} Adrienne L. Norris,[§] Jerome Baudry,^{*,†,§} and Engin H. Serpersu^{*,§}

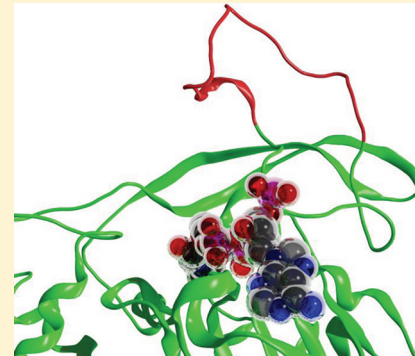
[†]UT/ORNL Center for Molecular Biophysics, Oak Ridge National Laboratory, Oak Ridge, Tennessee 37830, United States

[‡]Graduate School of Genome Science and Technology, University of Tennessee, Oak Ridge, Tennessee 37830, United States

[§]Department of Biochemistry and Cellular and Molecular Biology, University of Tennessee, Knoxville, Tennessee 37996, United States

Supporting Information

ABSTRACT: NMR spectroscopy experiments and molecular dynamics simulations were performed to describe the dynamic properties of the aminoglycoside acetyltransferase (3)-IIIb (AAC) in its apo and coenzyme A (CoASH) bound forms. The ¹⁵N-¹H HSQC spectra indicate a partial structural change and coupling of the CoASH binding site with another region in the protein upon the CoASH titration into the apo enzyme. Molecular dynamics simulations indicate a significant structural and dynamic variation of the long loop in the antibiotic binding domain in the form of a relatively slow (250 ns), concerted opening motion in the CoASH-enzyme complex and that binding of the CoASH increases the structural flexibility of the loop, leading to an interchange between several similar equally populated conformations.



Antimicrobials (AG)-based antibiotics are used to treat infections caused by both Gram-positive and Gram-negative bacteria. These antibiotics bind to the 30S subunit of the prokaryotic ribosome and interrupt the bacterial protein synthesis.¹ However, the clinical effectiveness of these drugs is threatened due to emerging resistance to their action.² The main resistance mechanism is the enzymatic covalent modification of the AG, which causes a strong decrease in the AG's binding affinity to the prokaryotic ribosome.³ One enzyme that can covalently modify AGs is the aminoglycoside acetyltransferase(3)-IIIb (AAC), which transfers an acetyl group donated by the cofactor acetyl-CoA to the 3-N position on the central 2-deoxystreptamine ring (2-DOS).⁴ AAC has a very broad substrate spectrum and is one of the most promiscuous aminoglycoside-modifying enzymes (AGME).⁵ Homology modeling studies indicated that this enzyme belongs to the GNAT superfamily^{4,6} and that the antibiotic binding domain (motif B) contains a large, flexible loop (residues 66–101, blue segment in Figure 1a,b). This loop is 35 residues long and contains 14 charged residues (5 Arg, 5 Asp, and 4 Glu). Flexibility of another highly promiscuous AGME, the aminoglycoside phosphotransferase (3)-IIIa, has been described to be involved in the mechanism of its broad substrate promiscuity.⁷ Likewise, the flexible loop in AAC could possibly be involved in this enzyme's promiscuity.^{4,5}

Because of substrate overlap among many AGMEs, the development of new drugs to overcome the antibiotic resistance toward aminoglycosides requires a detailed understanding of ligand-enzyme interactions with several highly promiscuous

members of AGMEs. The presence of the cofactor, CoASH, has been previously shown to significantly increase the binding affinity of aminoglycosides to the AAC. The more favorable Gibbs free energy of antibiotic binding observed in the ternary complex is the result of an increase in favorable enthalpic contributions, which compensate the increase in unfavorable entropic contribution.⁵ However, binding of different substrates exhibits a diverse set of individual kinetic and thermodynamic properties even for structurally similar aminoglycosides such as neomycin and paromomycin.⁴ The rationalization of the molecular basis of these differences in thermodynamics of enzyme-ligand complexes requires an understanding of the enzyme structure and dynamics in the atomic resolution, such as obtained from the integration of NMR and molecular simulation approaches.

MATERIALS AND METHODS

NMR Spectroscopy. Uniformly enriched ¹⁵N-AAC was purified as in ref 5 from cells grown in M9 minimal media with ¹⁵NH₄Cl. Amino acid-specific labeled AAC was also prepared in the same manner except that each amino acid was added individually in the M9 minimal media with only the amino acid of interest (¹⁵N-Ala or ¹⁵N-Leu in this case) being ¹⁵N-enriched. The NMR sample contained 230 μM ¹⁵N-AAC in 50 mM Tris-HCl pH 7.6 with 100 mM NaCl at 25 °C. Sensitivity-enhanced ¹⁵N-¹H HSQC spectra

Received: June 30, 2011

Revised: October 25, 2011

Published: October 25, 2011

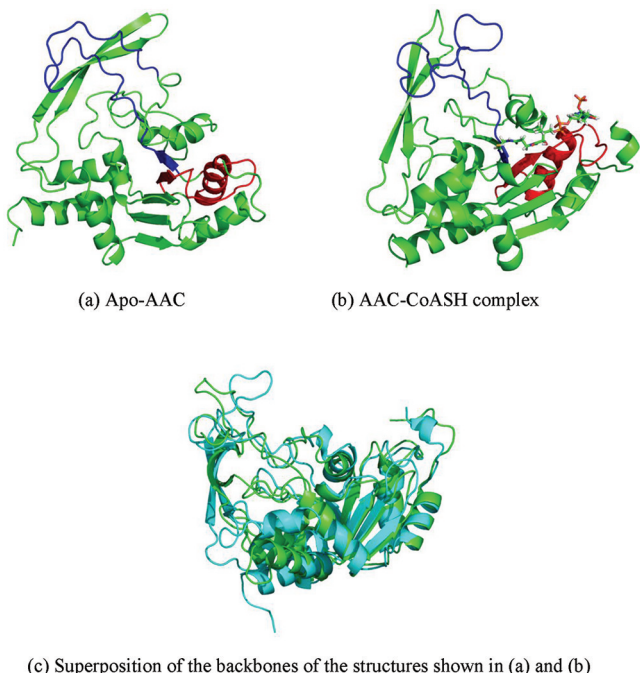


Figure 1. Initial structures for the MD production runs: the apo enzyme (a) and the CoASH-enzyme complex (b) are shown in the “cartoon” representation, and the CoASH is shown in the “sticks” representation. In each figure, the conserved antibiotic binding motif (loop-*b*-strand, residues 27–58) is colored in blue, and the conserved CoASH binding structural motif (strand-loop-*a*-helix, residues 61–94) is colored in red. (c) Superposition of the peptide backbone of the initial structures of apo enzyme (green) and the CoA-complex (cyan); the average RMSD between these two structures is 1.62 Å.

(will be referred as HSQC henceforth) provided by the standard Varian software (VNMRJ) based on the pulse sequence described in ref 22 with TROSY option²³ were acquired on a 600 MHz Varian INOVA equipped with a salt tolerant, cryogenic probe. Spectra were acquired with 64–128 transients and 64 s dimension increments. Data were processed with nmrPipe⁸ and displayed by SPARKY software.⁹ Substrate titrations were performed by adding concentrated CoASH directly to the enzyme solution. HSQC spectra were acquired after each addition to identify changes in the spectrum as a function of CoASH binding to the enzyme.

Molecular Dynamics Simulations Setups. Three independent simulation systems were built: (I) apo-species of the enzyme based on the homology structure by Norris et al.,⁴ (II) enzyme–CoASH complex, and (III) apo enzyme species obtained from the direct removal of CoASH from system II after equilibration (i.e., systems II and III have identical initial structures at the beginning of the MD production run, but II contains CoASH, while III does not).

For system II, the CoASH was included in the protein structure using the program MOE²¹ by superimposing the homology model used in system I with the X-ray crystal structure of the aminoglycoside N3-acetyltransferase from *Bacillus anthracis* (PDB entry 3IJW). This protein shares >25% sequence identity and >60% similarity to AAC and was one of the template proteins used in the development of the homology model.⁴ The simulated AAC model (full-length protein with 274 residues) consists of 4073 protein atoms.

The AMBER ff99sb force field parameters¹⁰ were used for the protein in all systems while the force field parameters for CoASH were obtained from the AMBER general force field (GAFF)¹¹

using the program ANTECHAMBER¹² from the AMBER tool package (version 1.4). All three systems are explicitly solvated using TIP3P water molecules¹³ in a cubic simulation box of $8\text{ nm} \times 8\text{ nm} \times 8\text{ nm}$, leading to a total atom number of about 50 000. All three systems were first subject to an energy minimization of 10 000 steps using the steepest decent algorithm, followed by an equilibration stage in the NTP thermodynamic ensemble (constant particle number, temperature, and pressure) at 300 K and 1 bar pressure for 5 ns, using the Nosé-Hoover temperature control algorithm^{14,15} and the Berendsen weak coupling pressure control algorithm.¹⁶ Another 10 ns equilibration was carried out in the same ensemble with the same temperature and pressure but with the Berendsen pressure control replaced by the Panirello–Rahman algorithm,¹⁷ which is also used in the subsequent production runs, to ensure correct thermodynamics ensemble properties.¹⁸ After the second equilibration, 0.5 μs long production runs were carried out for each of the three simulation systems, leading to 1.5 μs total simulation time. A 2 fs integration time step was used for both equilibration and production runs, and the atomic coordinates were saved into the trajectory every 10 ps. All minimization, equilibration, and production runs were performed with the GROMACS MD simulation engine (version 4.0.7).¹⁹ The last 300 ns of the production runs, exhibiting converged backbone C α root-mean-square deviation (RMSD) (with respect to the initial structure of the production run), was used for analysis. Details about the analysis are available in the Supporting Information.

■ RESULTS AND DISCUSSION

CoASH Interaction with AAC Implies Dynamics Variations of Certain Residues. The full NMR HSQC spectrum of apo-AAC shows about 200 resonances of this 274 amino acid enzyme.⁵ AAC contains 20 proline residues, which are invisible in the HSQC spectrum; however, the AAC spectrum is missing about 50 additional resonances. These are likely to represent resonances that fall into an intermediary exchange regime between two or more conformations of the peptide backbone and are consequently undetectable due to line broadening. These observations are consistent with the data from homology modeling⁴ and independent bioinformatics analysis (Supporting Information, section 1, Figures S1 and S2) of the enzyme, where the AG binding loop (residues 66–101) is suggested to be unstructured. The missing resonances may belong to residues in this site and/or to the flexible N- and C-termini of AAC. Additional experimental evidence supporting these conclusions were obtained by acquiring HSQC spectra with selectively enriched AAC. The first of these is ¹⁵N-Leu-enriched AAC. As shown in Figure S4a, 28–29 cross-peaks representing almost all of the 29 leucines of AAC are visible in the HSQC spectrum. Contrary to this, about 8–9 of the expected 39 cross-peaks are missing from the spectrum of ¹⁵N-Ala enriched AAC (Figure S4b). These observations are consistent with the expected dynamic behavior of the protein. There are three alanine residues in the N-terminus and four are on the AG binding loop. The missing cross peaks are likely to belong to these residues. Contrary to this, there is no leucine at either terminus and only one is located in the AG binding loop (Leu 75). Thus, the data strongly suggest that these cross-peaks are missing due to dynamic properties of the backbone segment that they are located rather than being masked by other cross-peaks in the crowded region of the spectrum.

Titration with substrates also provided evidence for the dynamic behavior of the enzyme. Addition of CoASH to AAC causes changes in the dynamic behavior of a number of residues

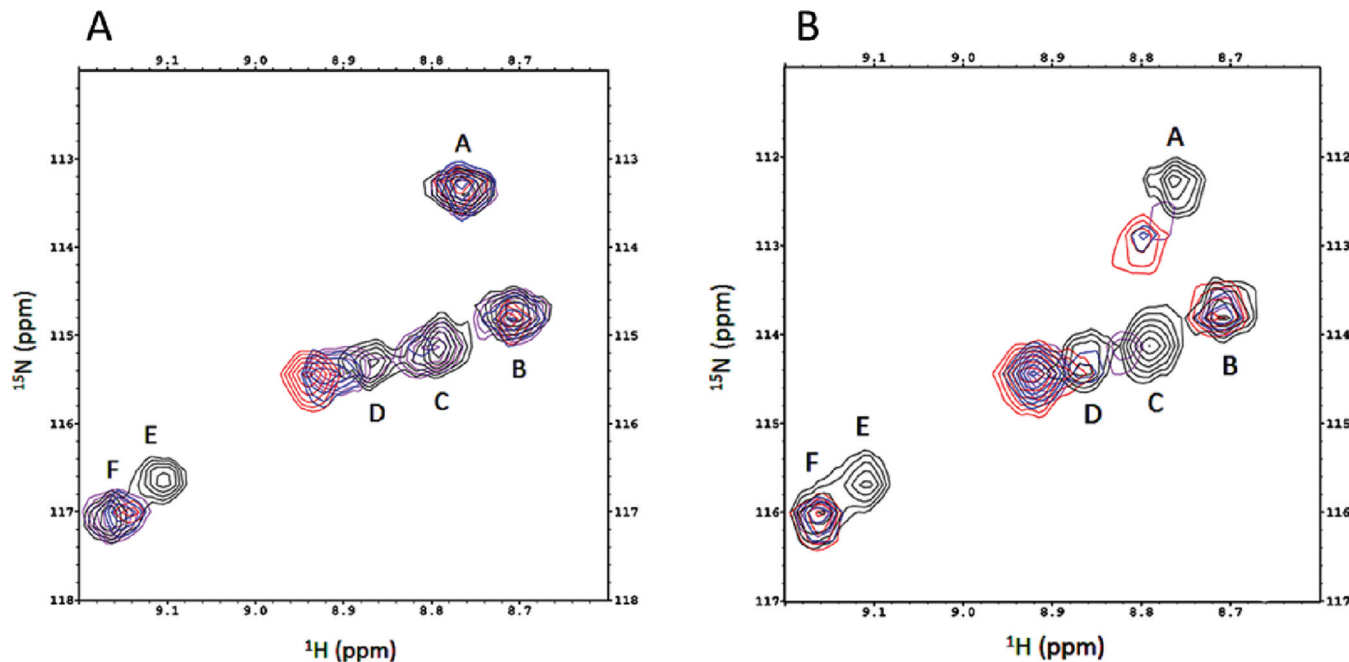


Figure 2. Shown here is an expanded view of a region of the HSQC spectrum in which several ¹⁵N-¹H correlation peaks from uniformly ¹⁵N-enriched AAC respond to CoASH (panel A) or aminoglycoside antibiotic (panel B) titration. The full spectrum is provided in the Supporting Information. Black peaks correspond to the unliganded form of AAC with increasing concentrations of either CoASH or antibiotic overlaid from levels of partial to full saturation of the binding sites (purple to blue to red). All spectra are shown at the same level of contour.

such that some (~26) disappear from the HSQC spectrum (peak E in the left panel of Figure 2) while others (~10) undergo concentration-dependent line broadening (peaks A and C). CoASH has a strong affinity to the enzyme where the dissociation constant of the binary AAC-CoASH complex, determined by NMR, fluorescence, and ITC yielded values ranging from 1.5 to 3.8 μM .⁵ Thus, the tight binding of CoASH to the enzyme strongly suggests that the broadening observed in these cross-peaks are not due to transient binding and dissociation of CoASH because it is unlikely that CoASH would be in fast exchange under these conditions. We should also indicate that the binding of CoASH to AAC is enthalpically disfavored and entropically favored yielding a net favorable Gibbs energy for the formation of the complex (i.e., entropy-driven).⁵ Although a favorable entropic contribution can be from different sources such as release of water molecules upon ligand binding, it is also consistent with increased freedom of mobility of the AG binding loop. Furthermore, some of the peaks (>15) affected by CoASH binding are similarly perturbed by antibiotic titration (Figure 2, right panel), indicating that the binding of CoASH at the CoASH binding site may trigger structural rearrangement of the protein backbone in the substrate binding region or vice versa. Since these perturbations involve broadening of peaks even with the tightest binding aminoglycoside neomycin ($K_D \leq 0.6 \mu\text{M}$), it provides further support to the previous suggestion that the broadening observed in some resonances represents changes in dynamic behavior of these residues rather than exchange broadening due to ligand binding and dissociation. Such differences are also observed between the complexes of different antibiotics regardless of the tightness of the binding, which is again consistent with the ligand-dependent changes in protein dynamics. Such behavior appears to be common with aminoglycoside modifying enzymes because we also observed similar aminoglycoside-dependent spectral changes in dynamic properties of a different enzyme, the aminoglycoside phosphotransferase(3)-IIIa.^{7,24} Previous data acquired by isothermal

titration calorimetry (ITC) indicated that CoASH is able to increase antibiotic binding affinity to AAC in an antibiotic-dependent manner that varies from 4-fold up to 15-fold,⁵ providing additional evidence that there is a link between these two distinct ligand binding sites. It is likely that binding of CoASH to AAC causes conformational changes in the aminoglycoside binding site, which also affects dynamic properties of some backbone amides. Together, these findings suggest that CoASH alters dynamic properties of residues in the AG binding site to render binding of structurally diverse antibiotics to AAC thermodynamically more favorable. This is, again, similar to what is observed the aminoglycoside phosphotransferase(3)-IIIa²⁵ where binding of Mg-nucleotide increases the mobility of the residues on the AG binding site. Since the aminoglycoside phosphotransferase(3)-IIIa has even a broader substrate specificity than AAC, it appears that this mode of action may be the mechanism of achieving substrate promiscuity in the aminoglycoside modifying enzymes.

CoASH Binding Induces Increased Backbone Dynamics and Structural Fluctuations of the Loop Region. The root-mean-square fluctuation (RMSF) of the backbone Ca atoms for all three simulation systems with respect to the protein average structure are shown in Figure 3a. Figure 3a shows that the residues in the loop region of the CoASH complex exhibit higher fluctuations compared to the same residues in the apo and CoASH-deleted systems.

A principal component analysis (PCA) was performed to identify different “principal (eigen)motions” that contribute to the otherwise complex global protein dynamics. The most important contribution to the collective, global motions originates from the first few eigenmotions, considered to be essential for the biological functions of the protein.²⁰ The all atom covariance matrix and its eigenvalues and eigenvectors were calculated as described in the Supporting Information. The results for the first 20 eigenvalues are shown in Figure 4a. A graphical illustration of the motions corresponding to the 20 most dominant eigenvalues for each system is shown in

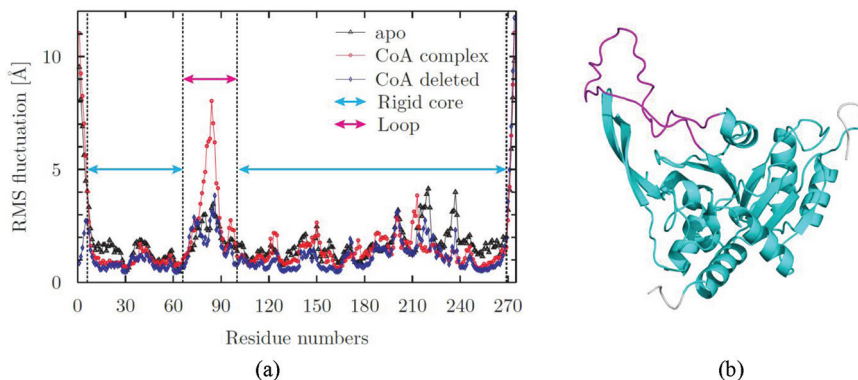


Figure 3. (a) Comparison of the root-mean-square fluctuation (RMSF) between different systems. The protein is divided into the loop and a “rigid core” part due to differences in the dynamics and presence (or absence) of a well-defined secondary structure. (b) Illustration of the loop part and the “rigid core” as a 3D structure. The loop is colored with magenta, and the rigid core is colored with cyan. The termini residues are colored in gray.

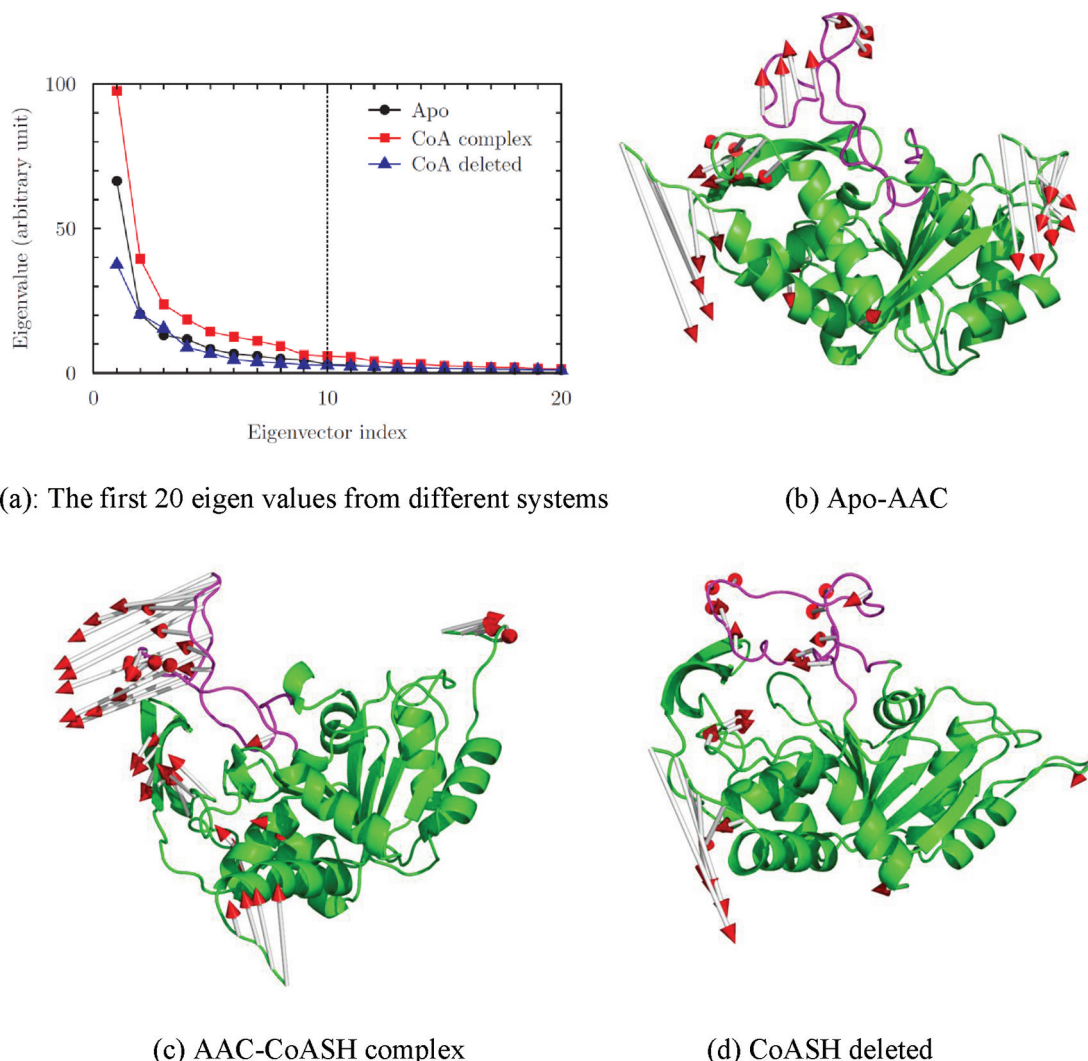
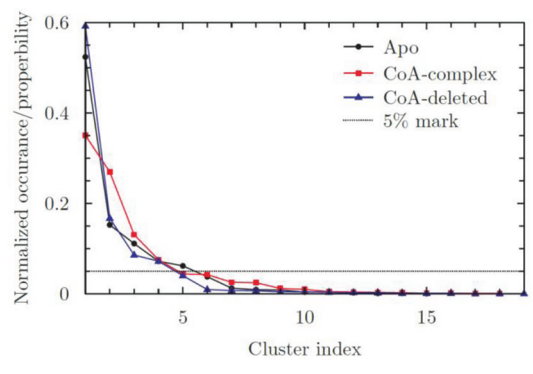


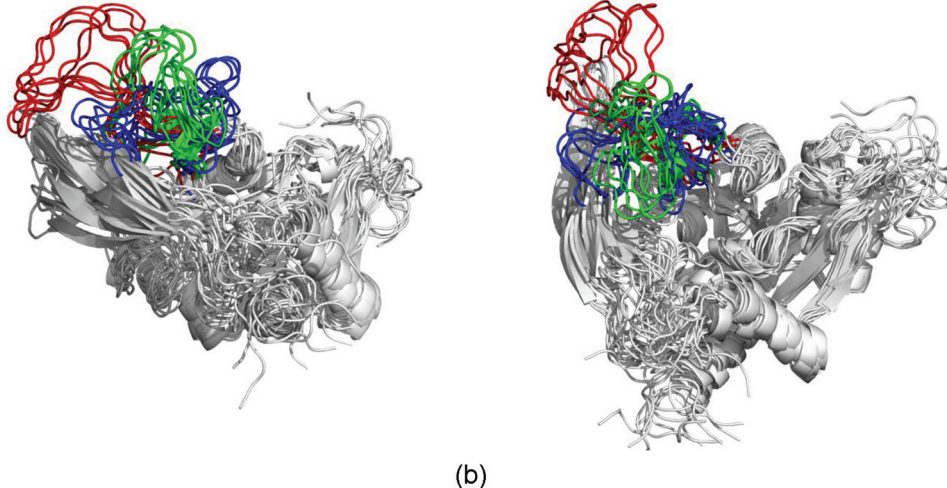
Figure 4. Principal motions of the protein backbone obtained from the projection of the trajectory of each system on their respective first 10 eigenvectors calculated from the PCA. The first 20 eigenvalues of different simulation systems are shown in (a); the dashed line at eigenvector index 10 is plotted as a visual aid. The motions are illustrated by arrows pointed from the C α atoms to the direction of the motions, and the length of the arrow is proportional to the magnitude of the motion. The loop region is colored in magenta. The loop in the CoA complex (c) carries out a large concerted “opening motion” while the loops in the apo and CoA-deleted systems (b and d, respectively) move rather randomly with significantly smaller amplitudes.

Figure 4b,c. The arrows are pointing to the direction of the motion of the respective C α atoms. The length of the vector is proportional to the magnitude of the motion it represents.

In all three systems, the motions of the rigid core regions are marginal outside of the termini. Larger amplitude motion originates from the loop region, in agreement with the RMSF



(a)



(b)

Figure 5. The diagram (a) shows the normalized relative occurrence of clusters in different systems indexed by the cluster population. A 5% mark is plotted as a visual aid. (b) illustrates the superposition of the first 5 most dominant structures from the 3 different simulation systems (therefore total 15 structures) viewed from 2 different perspectives. The loop regions of the structures from different systems are colored differently: green = apo, red = AAC-CoASH complex, blue = CoA-deleted.

results shown in Figure 3a. However, the dynamics of the loop in the CoASH complex is different than those in the CoASH-free systems. In the CoASH complex, the loop performs a concerted large “opening” motion, on a time scale of about 250 ns, while the motions of the loops in the apo and CoASH-deleted systems exhibit smaller magnitudes without systematic concerted directions. The magnitudes of different essential motions in different systems are also described by Figure 4a, since a given eigenvalue is proportional to the mean-square fluctuation of the respective principal motion. Figure 4a shows that the first 10 eigenvalues of the CoASH complex are higher than those of the apo and CoASH-deleted systems. The first 10 eigenvalues of the apo and CoASH-deleted systems are similar to each other except in the first eigenvalue, suggesting that the magnitudes of the second to tenth principal modes of motions in these two systems do not differ systematically. Together, these results indicate that CoASH binding to AAC induces higher backbone fluctuations in the loop region than in the case of the apo-species, through a relatively large concerted motion of the loop.

Dominant Loop Structures Are Different in the CoASH Complex. A clustering analysis of the trajectories was performed using the algorithm described in the Supporting Information (section 3) using the all-atom RMSD as metric. To provide a qualitative description of the loop structure, the RMSD was calculated by superimposing the backbone C α

atoms of the rigid core. The clustering analysis algorithm yields a series of nonoverlapping conformational clusters that represent a conformational substate and a cluster population proportional to the occupation probability for the corresponding conformation. Using an all-atom RMSD cutoff of 1.3 Å, 15, 18, and 19 clusters were found for the apo, CoASH complex, and CoASH-deleted system, respectively. The corresponding structures are superimposed and are shown in Figure 5b. The main difference between structures from different systems originates in differences in the loop structures. In the CoASH complex, the loops are more opened and stretched away from the center cavity of the protein. In both, the apo and CoASH-deleted systems, the loop structures are not exactly identical but do share some similar characteristics: in both cases, the loop is folded more tightly than the loop of the CoASH complex and remains closer to the folded core of the protein. The distinct differences in dominant structures between the CoASH-bound and CoASH-free systems suggest that CoASH binding induces a change in the conformation of the loop, in addition to the dynamics changes as shown in Figure 4.

The normalized populations of different clusters are shown in Figure 5a, where different clusters are indexed by the population of conformations within each cluster; i.e., the largest cluster is indexed as 1, the second largest 2, and so on. There is a particularly dominant cluster in both apo and CoASH-deleted

systems, populated between 50% and 60% of the total analyzed simulation time. The second largest clusters are populated 15–20% of the time. However, in the case of the CoASH complex, the largest cluster is only occupied about 35% of the time and about 27.5% for the second largest cluster. The time dependency of the occupation of different clusters is shown in Figure S3 of the Supporting Information for each of the three simulated systems, where the *y*-axes indicate the cluster index (same indexing as in Figure 5a). Figure S3 shows that in both apo and CoASH-deleted simulations (i.e., Figure S3a,c) the majority of transitions between different conformation clusters are transitions from and to the dominant structural cluster (index 1). However, in the CoASH complex system, the transitions between clusters imply three clusters (index 1–3) with a similar population. These results suggest that the loop conformation in the CoASH complex switches between several different conformations with similar free energy rather than predominantly occupying one particular conformation, i.e., like in the case of the apo-species.

The binding of the CoASH significantly alters the protein surface around the aminoglycoside binding site. In Figure 6, we

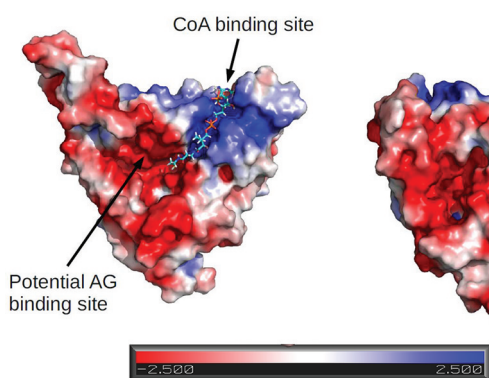


Figure 6. Average structures of the AAC–CoASH complex (left) and apo AAC (right) obtained from the last 100 ns of the simulation trajectories. CoA is shown in the “sticks” representation. Coloring represents the electrostatic potential along the protein van der Waals surface; color scales range from −2.5 (red) to +2.5 (blue) $k_B T/e$, where k_B is the Boltzmann constant, $T = 300$ K is the temperature, and e is the elementary charge.

compared the average structures of the apo-AAC and AAC–CoASH complex calculated from the last 100 ns of the respective simulation trajectories, which should provide a good representation of the final structures of the simulations. The protein structures are illustrated in the van der Waals surface representation, and the coloring is based on the electrostatic surface potential calculated with the adopted Poisson–Boltzmann solver (APBS) package.²⁶ In the CoASH bound form, putative substrate binding site takes a form of a negatively charged cavity that has a significantly wider opening and also more shallow than that of the apo enzyme, where the cavity is deeper and also has a significantly smaller opening. This structural difference of the potential substrate binding site is caused by the conformational change of the loop in the CoA complex as described above. This finding is in agreement with the experimental observation that the aminoglycoside binding affinity increases if CoASH is bound to the enzyme, since a shallower and negatively charged cavity with a wider opening may allow positive substrates to find the binding site more efficiently during the diffusion process.

CONCLUSIONS

The NMR experiments and MD simulations presented here suggest spatially anisotropic protein dynamics that differ between the apo- and CoASH-bound species. The tertiary structure of the protein can be divided into a rigid core region (residues 6–65 and residues 102–269) and flexible loop region (residue 66–101) based on different RMSF values. The rigid core has, in general, well-defined secondary structures. The loop region (residues 66–101), in contrast, lacks a well-defined secondary structure and exhibits RMSFs over the course of the MD simulations that are higher in the AAC–CoASH complex than in the apo-species. The loop region located in the substrate binding motif undergoes a concerted opening motion in the CoASH-bound species, apparently moving away from the antibiotic binding site. The conformational change of the loop caused by the CoASH binding creates a larger opening of the cavity and also decreases its depth simultaneously. Increased flexibility of this loop may also aid in binding of structurally diverse aminoglycosides to AAC to be thermodynamically more favorable. This conformational change is not observed in the apo-species. The clustering analysis indicated that the loop in the antibiotic binding motif occupies several similarly populated and relatively long-lived conformations (50–100 ns) in the CoASH complex rather than one dominant conformation as in the apo-species. While the MD simulations performed here are about 3 orders of magnitude faster than the time scale investigated by the NMR experiments, the simulation suggests possible dynamics and structural differences of AAC upon binding of the coenzyme that are in agreement with the increased flexibility of the complex observed in the NMR experiments. It will be interesting to investigate the AAC loop dynamics further on slower time scales, possibly using coarse-grained molecular dynamics simulations, to describe the structural changes induced by coenzyme binding.

ASSOCIATED CONTENT

Supporting Information

Protein sequence, folding statistical analysis, details of the principal component analysis and clustering analysis, as well as time series of cluster population in the simulated models. This material is available free of charge via the Internet at <http://pubs.acs.org>.

AUTHOR INFORMATION

Corresponding Author

*E-mail jbaudry@utk.edu, Ph 1-865-574-6308, Fax +1 865 576 7651 (J.B.). E-mail serpersu@utk.edu, Ph 1-865-974-2668 (E.H.S.).

Funding

This work is supported by a grant from the National Science Foundation (MCB-0842743 to EHS). X.H. is supported by the Genome Science and Technology graduate program of the University of Tennessee, Knoxville, TN. A.L.N. is partly supported by the U.S. Department of Energy EPSCoR Implementation award (DE-FG02-08ER46528). J.B. is supported by the University of Tennessee, Knoxville, TN.

ACKNOWLEDGMENTS

We thank Xiaolin Cheng from Oak Ridge National Laboratory for fruitful discussions and the University of Tennessee/Oak Ridge National Laboratory Center for Molecular Biophysics for computing resources.

ABBREVIATIONS

AAC, aminoglycoside acetyltransferase (3)-IIIb; CoA/CoASH, coenzyme A; 2-DOS, 2-deoxystreptamine; AGME, aminoglycoside-modifying enzymes; HSQC, heteronuclear single quantum coherence; MD, molecular dynamics; PCA, principal component analysis.

REFERENCES

- (1) Moazed, D., and Noller, H. F. (1987) Interaction of antibiotics with functional sites in 16S ribosomal RNA. *Nature* 327, 389–394.
- (2) Yamane, K., Wachino, J., Doi, Y., Kurokawa, H., and Arakawa, Y. (2005) Global spread of multiple aminoglycoside resistance genes. *Emerging Infect. Dis.* 11, 951–953.
- (3) Lorian, V. (1991) Aminoglycoside-Aminocyclitol Antibiotics and Their Modifying Enzymes. Antibiotics in Laboratory Medicine, in *Antibiotics in Laboratory Medicine*, 4th ed. (Davis, J. E., Ed.), p 1283.
- (4) Norris, A. L., Özen, C., and Serpersu, E. H. (2010) Thermodynamics and Kinetics of Association of Antibiotics with the Aminoglycoside Acetyltransferase (3)-IIIb, a Resistance-Causing Enzyme. *Biochemistry* 49, 4027–4035.
- (5) Norris, A. L., and Serpersu, E. H. (2010) Interactions of Coenzyme A with the Aminoglycoside Acetyltransferase (3)-IIIb and Thermodynamics of a Ternary System. *Biochemistry* 49, 4036–4042.
- (6) Neuwald, A. F., and Lansman, D. (1997) GCN5-related histone N-acetyltransferases belong to a diverse superfamily that includes the yeast SPT10 protein. *Trends Biochem. Sci.* 22, 154–155.
- (7) Norris, A. L., and Serpersu, E. H. (2009) NMR Detected Hydrogen-Deuterium Exchange Reveals Differential Dynamics of Antibiotic- and Nucleotide-Bound Aminoglycoside Phosphotransferase (3)-IIIa. *J. Am. Chem. Soc.* 131, 8587–8594.
- (8) Delaglio, F., Grzesiek, S., Vuister, G. W., Zhu, G., Pfeifer, J., and Bax, A. (1995) Nmrpipe - a Multidimensional Spectral Processing System Based on Unix Pipes. *J. Biomol. NMR* 6, 277–293.
- (9) Goddard, T. D., and Kneller, D. G. SPARKY 3. <http://www.cgl.ucsf.edu/home/sparky/>.
- (10) Hornak, V., Abel, R., Okur, A., Strockbine, B., Roitberg, A., and Simmerling, C. (2006) Comparison of multiple Amber force fields and development of improved protein backbone parameters. *Proteins* 65, 712–725.
- (11) Wang, J., Wolf, R. M., Caldwell, J. W., Kollman, P. A., and Case, D. A. (2004) Development and testing of a general amber force field. *J. Comput. Chem.* 25, 1157–1174.
- (12) Wang, J., Wang, W., Kollman, P. A., and Case, D. A. (2006) Automatic atom type and bond type perception in molecular mechanical calculations. *J. Mol. Graphics Modell.* 25, 247260.
- (13) Jorgensen, W. L., Chandrasekhar, J., Madura, J. D., Impey, R. W., and Klein, M. L. (1983) Development and testing of a general amber force field. *J. Chem. Phys.* 79, 926–936.
- (14) Nosé, S. (1984) A unified formulation of the constant temperature molecular dynamics methods. *J. Chem. Phys.* 81, 511–520.
- (15) Hoover, W. G. (1985) Canonical dynamics: Equilibrium phase-space distributions. *Phys. Rev. A* 31, 1695–1697.
- (16) Berendsen, H. J. C., Postma, J. P. M., van Gunsteren, W. F., DiNola, A., and Haak, J. R. (1984) Molecular dynamics with coupling to an external bath. *J. Chem. Phys.* 81, 3684–3691.
- (17) Parrinello, M., and Rahman, A. (1981) Polymorphic transitions in single crystals: A new molecular dynamics method. *J. Appl. Phys.* 52, 7182–7190.
- (18) Bussi, G., Donadio, D., and Parrinello, M. (2006) *J. Chem. Phys.* 126, 014101.
- (19) Hess, B., Kutzner, C., van der Spoel, D., and Lindahl, E. (2008) GROMACS 4: Algorithms for Highly Efficient, Load-Balanced, and Scalable Molecular Simulation. *J. Chem. Theory Comput.* 4, 435–447.
- (20) Tournier, A. L., and Smith, J. C. (2003) Principal Components of the Protein Dynamical Transition. *Phys. Rev. Lett.* 91, 208106.
- (21) Molecular Operating Environment (MOE), version 2010, The Chemical Computing Group, Montreal, Canada.
- (22) Kay, L. E., Keifer, P., and Saarinen, T. (1992) Pure absorption gradient enhanced heteronuclear single quantum correlation spectroscopy with improved sensitivity. *J. Am. Chem. Soc.* 114, 10663–10665.
- (23) Weigelt, J. (1998) Single scan, sensitivity- and gradient-enhanced TROSY for multidimensional NMR experiments. *J. Am. Chem. Soc.* 120, 10778–10779.
- (24) Serpersu, E. H., Özen, C., Norris, A. L., Steren, C., and Whittemore, N. (2010) Backbone resonance assignments of a promiscuous aminoglycoside antibiotic resistance enzyme; the aminoglycoside phosphotransferase(30)-IIIa. *Biomol. NMR Assignments* 4, 9–12.
- (25) Wieninger, S. A., Serpersu, E. H., and Ullmann, G. M. (2011) ATP Binding Enables Broad Antibiotic Selectivity of Aminoglycoside phosphotransferase(3')-IIIa: An Elastic Network Analysis. *J. Mol. Biol.* 409, 450–465.
- (26) Baker, N. A., Sept, D., Joseph, S., Holst, M. J., and McCammon, J. A. (2001) Electrostatics of nanosystems: Application to microtubules and the ribosome. *Proc. Natl. Acad. Sci. U. S. A.* 98, 10037–10041.